Lisbon, October 22th 2015

Potential analysis of Additive Manufacturing technique

Silva, Frederico Miguel Ferreira.da

Técnico Lisboa, Av. Rovisco Pais, 1200 Lisboa, Portugal

Abstract

Nowadays the manufacturing processes are highly dependent on the machining operations to remove material up to the final shape. In modern industry all measures are taken to manufacture products in a sustainable perspective, taking in consideration the low manufacturing cost and environmental issues in account.

Therefore, 3D printing has been analyzed from a perspective of industrialization, especially in the production of metallic components. The welding techniques are the key solution in implementing 3D printing processes.

Power sources such as laser and electron beam are used for additive manufacturing but in the perspective of industrialization. Electric arc welding technology has been developed and implemented in industry long ago and presents higher deposition rates compared to laser and electron beam power sources with lower investment costs.

In this work, the GMAW process was used due to the fact that it is a process widely used industrialized due to its efficiency and existing variants. The consumable used in this work is ER 5356, equivalent to the 5083 aluminum alloy. The variant studied was Cold Metal Transfer (CMT) which has emphasis in several works in the field of Additive Manufacturing due to the ability to operate with low heat input. Deposition efficiency, heat input, useful material ratio, hardness, metallographic and nondestructive testing were the aspects studied as indicators of analysis potential of additive manufacturing, using this technique.

Keywords: 3D Printing, Additive Manufacturing, CMT (Cold Metal Transfer), Aluminium alloy 5083, Deposition efficiency, metallography

1. Introduction

Additive Manufacturing (AM) is a fabrication method which consists on overlapping successive layers of material. The output is a three dimensional (3D) finished or near finished part. This manufacturing method does not appear in the history as that, but instead, it is introduced as a Rapid Prototyping (RP)

process in the 1980's, with the objective of creating models of parts [1]. In this work the AM processes addressed regard metallic materials since the use of AM technologies for producing metal parts is growing rapidly and migrating from a technique used for manufacturing parts in high value raw materials, such as titanium and its alloys, to other materials as aluminium, steel and respective alloys. At the manufacturing of some metals is difficult and expensive, it is important to minimize the waste rate of the traditional manufacturing processes. Metal Additive Manufacturing is a technique that can produce 3D parts with the main advantage that allows skipping some steps in the manufacturing process. The main concern of the use of MAM technologies is to guarantee that the final properties of the part produced are as good as the base material and that the required dimensional requirements are fulfilled.

The AM processes can be classified regarding its characteristics such as: feeding system, energy source and deposition rate (Figure 2). [2]. With this evolution, the manufacturing technologies used in AM are also changing in comparison with conventional technologies as welding, with laser and electron beam.

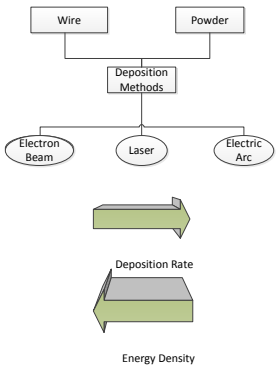

Figure 1: Schematic representation of Layer Manufacturing (LM) for metals.

In this work, a Wire and Arc Additive Manufacturing (WAAM) technique was used. This process combines the electric arc as power source with a wire feeding system, to create parts layer by layer.

Among arc welding processes, Gas Metal Arc Welding (GMAW), shown in Figure 3, has been adopted through this work since has significant advantages. It can weld all types of metals and alloys, it can weld in all positions, it does not have the same restrictions in electrode dimensions when compared with shielded metal arc welding, has higher welding speeds as high deposition rate and is extensively used in the industry these days.

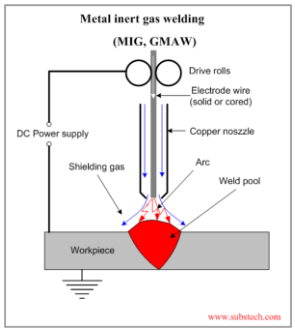

Figure 1 – GMAW process scheme.

GMAW processes adapt through time in order to improve the productivity of the process and the quality of the weld itself. In order to achieve that directive, *Fronius* introduced a new variation of the GMAW process called CMT. CMT is characterized by low heat input compared to the conventional GMAW, producing free spatter welds combined with low dilution of the base material [3]. Figure 3 shows a scheme of this process.

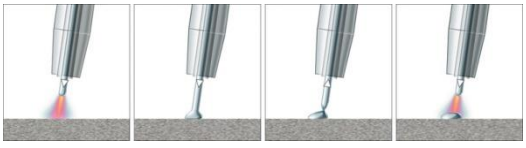

Figure 2 – CMT process scheme.

The CMT process has two major phases, the arcing phase and the short circuit phase, shown Figure 4 [4].

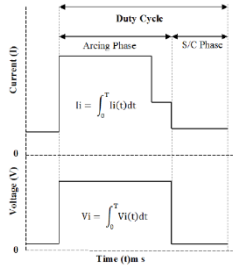

Figure 3 – CMT welding phases.

The CMT operation mode consists in four stages.

In stage one, the wire move towards the workpiece and the arc is formed, due to the increase of the voltage. The significant current increase as well.

During stage two the droplet is formed and the wire reverses its motion associated with the arc extinction. In this phase the weld pool is formed.

Stage three consists in the wire retraction, detaching the droplet in to the workpiece. The voltage drops to values near zero.

Finally, in stage four, is the stage and the beginning of a new operation cycle, the wire motion reverses again and the arc is reignited.

2. Experimental Approach

2.1. Materials and Welding parameters

Several samples obtained by multi-layer linear welds were built and compared. The equipment used for this experimental setup was:

- *Kuka* 6-axis robot system;
- *Fronius* CMT welding equipment + parameter controller;
- Welding wire consumable ESAB ER5356 with a diameter of 1mm;
- Substrate plates of Aluminium alloy 5083 with the dimensions of 300mm x 50 mm x 15mm;
- Clamping system;
- Argon shielding gas 99,9% atmosphere;
- National Instruments DAQ software + device;
- Voltage and current transducer;

For the robot trajectory was adopted a two way trajectory in the same direction.

2.2. Deposition Efficiency and Heat Input

The Deposition Efficiency and Heat Input were calculated and in this process the two ratios are directly dependent from each other. The Deposition efficiency is the ratio between the material deposited on the substrate plate and the welding wire fed for the process. The steps followed to determine the process efficiency were:

- Before the wall manufacturing, the substrate plates were all weighed;
- Build the walls;
- Remove the plates with the walls and weigh again;

After acquiring the data, this was treated in order to calculate the process efficiency and Heat Input by using the following equations:

- Weight of electrode used (WEU):

$$WEU(g) = WFS.A_e.l_e.\rho_e.t_w \quad (1)$$

- Deposition Efficiency (DE):

$$DE(\%) = \frac{mass_{before} - mass_{after}}{mass_{eletrode}} \times 100 \quad (2)$$

- Heat Input (HI):

$$HI(kJ/mm) = \frac{V \times I \times 60}{WS \times 1000} \times \eta_{MIG} \quad (3)$$

The efficiency of the GMAW welding process is considered 0.8 [4].

The process parameters used in this work are shown in table 1.

Current (A)	Voltage (V)	Wire Feeding Rate(m/min)	Travel speed (mm/min)	Gas Flow rate (L/min)	Torch Angle (degrees)	Stick-out length (mm)
130	17.6	11.4	600	17	0	15 -- 20
120	17.3	10.4	600	17	0	15 – 20
110	16.9	9.3	600	17	0	15 – 20
100	16.5	8.5	600	17	0	15 – 20
90	16	7.6	600	17	0	15 – 20
80	15.6	6.8	600	17	0	15 – 20
70	14.9	6.0	600	17	0	15 – 20
60	14.1	5.2	600	17	0	15 – 20

Table 1: Initial parameter setting defined for wall buildings

2.3. Macrostructure and Microstructure analysis

Macro and micro analysis imply destroying the AM walls to produce samples from the welded sections. These tests allow to estimate the Useful Mass Ratio (UMR), observing defects like poor fusion, porosity, inclusions and other metallurgical aspects like grain size and precipitates.

For the UMR calculations the equations used were:

$$UMR = \frac{m_{useful}}{m_{deposited}} \times 100\% \quad (4)$$

$$m_{deposited} = m_{substrate+deposit} - m_{substrate} \quad (5)$$

$$A_{useful} = w_{useful} \times h_{useful} \quad (6)$$

$$m_{useful} = (A_{useful} \times l_{wall}) \times \rho_{alloy} \quad (7)$$

$$UMR = \frac{m_{useful}}{m_{deposited}} \times 100\% \quad (8)$$

For the microstructure analysis was used the Light Optical Microscopy (LOM) analysis, in order to verify the success of the etching and calculate the average grain size with the Heyn method. After that, Scanning Electron Microscopy and Electronic Differential Scanning (SEM/EDS) was executed in order to analyze the microstructure in detail, especially if precipitates were formed and to obtain a chemical composition of those.

2.4. Hardness

A Vickers hardness test was performed. The test was performed using a load of 4,902N during 10 seconds. Twenty five indentations on each sample were performed along the build-up. The feature evaluated was the average hardness and the standard deviation from the average value.

2.5. Non Destructive Testing

In this work the Ultrassound Testing (UT) technique was tested in AM parts in order to evaluate the reliability of this technique using pulsed echo and PAUT. The results were confirmed further by a X-ray test.

The representation for the results of this test is the A-Scan [5].

3. Results and Discussion

3.1. Average current and voltage calculations

For both parameters the approach used to calculate the average values were the same that was [5]:

$$\bar{V} = \frac{\frac{t_1(V_p - V_b)}{2} + t_2(V_p - V_b) + \frac{t_3(V_p - V_b)}{2} + V_b(t_b + t_p)}{(t_b + t_p)} \quad (12)$$

$$\bar{I} = \frac{\frac{t_1(I_p - I_b)}{2} + t_2(I_p - I_b) + \frac{t_3(I_p - I_b)}{2} + I_b(t_b + t_p)}{(t_b + t_p)} \quad (13)$$

The equations used assume that the waveform has a trapezoidal form, and the expressions correspond to the area above the graph, meaning that:

$$V_i = \int_0^T V_i(t)dt \quad (14)$$

$$I_i = \int_0^T I_i(t)dt \quad (15)$$

The average values calculated for the wall build ups are expressed in the following table (Table 2):

Test Part	Current (A)	Voltage (V)	Travel speed (mm/min)	Wire Feeding Rate (m/min)	Gas Flow Rate (L/min)	Number of Layers
130A	166.2	23.4	600	11.4	17	20
120A	171.7	19.9	600	10.4	17	22
110A	135.7	20.2	600	9.3	17	22
100A	133.3	17.8	600	8.5	17	24
90A	110.9	15.9	600	7.6	17	24
80A	101.0	18.3	600	6.8	17	24
70A	85.3	15.2	600	6.0	17	26
60A	71.7	15.6	600	5.2	17	26

Table 2: Parameters obtained for each test part

3.2. Deposition Efficiency and Heat Input

The deposition efficiency determination is shown in the Table 3:

Test Part	Weight of electrode used (g)	Substrate plate weight (g)	Substrate plate + Deposit (g)	Deposition Efficiency (%)
130A	396.53	466.9	795.3	82.81
120A	397.92	456.2	797.7	85.82
110A	355.83	484.6	761.5	77.81
100A	354.79	472.9	742.7	76.04
90A	317.22	489.8	738.5	78.39
80A	283.83	461.3	691.4	81.06
70A	271.31	478.1	706.3	84.10
60A	235.13	504.9	698.4	82.29

Table 3: Deposition efficiency and weights used for its determination

For the Heat Input analysis the following table (Table 4) desbribes the parameters used and the results obtained:

Test Part	Current (A)	Voltage (V)	Travel speed (mm/min)	Heat Input (kJ/mm)
130A	166.2	23.4	600	0.311
120A	171.7	19.9	600	0.274
110A	135.7	20.2	600	0.220
100A	133.3	17.8	600	0.190
90A	110.9	15.9	600	0.141
80A	101.0	18.3	600	0.1487
70A	85.3	15.2	600	0.103
60A	71.7	15.6	600	0.089

Table 4: Heat Input values and parameter used for its determination

The values obtained allowed to build the graph that relates deposition efficiency and heat input, shown in Figure 5:

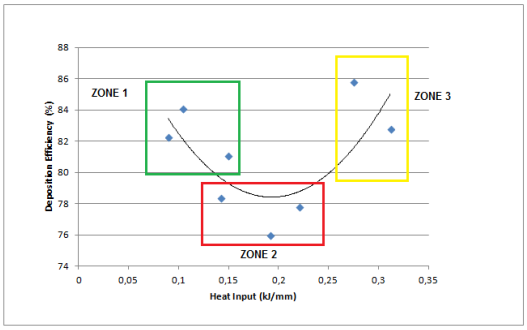

Figure 5: Relation between Deposition Efficiency and Heat Input

These values allow to distinguish 3 zones in Figure 5, the following can be considered:

- In the 1st Zone (green rectangle), the range of Values correspond to Currents between 70A and 100A, the metal transfer mechanism is characterized as short circuit transfer and the metal transfer it is stable allowing a smooth deposition of the droplets [3], this is an interesting operation domain to operate for AM;
- In the 2nd Zone (red rectangle), the Current range is between 110A and 135A, and the metal transfer mechanism is situated between the short circuit domain and the spray transfer domain [4], creating spatter and metal vaporization [3] [6], decreasing the deposition efficiency;
- In the 3rd zone (yellow rectangle), the range of values correspond to Currents between 165A and 170A and the transfer mode considered is the spray transfer, which means that the deposition efficiency is higher that the but the Heat Input it is higher too [5].

Considering these results, the best welding procedure to adopt in the fabrication of AM parts are the 70A set of parameters because reunites high deposition efficiency associated to a low heat input, allowing saving energy in the process and diminishing residual stresses.

3.3. Useful Mass Ratio

The macrostructure analysis in this work was performed in order to determine the useful cross section area in each test part and to establish an approach concerning the mass usage in an AM part, as described in the experimental procedure.

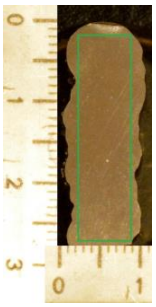

Figure 4 – Useful area represented for the 110A test part.

The results obtained on this procedure are expressed in Table 3:

Test Part	Useful Area (cm^2)	Useful mass (g)	Deposited Mass (g)	Weight of eletrode used (g)	UMR (%)
130A	2.12	140.45	328.4	396,53	42.7679659
110A	2.25	149.0625	276.9	397,92	53.83261105
80A	1.82	120.575	230.1	355,83	52.40112994
60A	1.56	103.35	193.5	354,79	53.41085271

Table 3: UMR calculations and values used for its calculation

Figure 7 shows the relation between UMR and heat input:

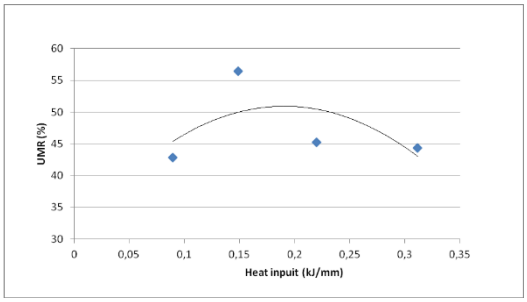

Figure 7: Relation between UMR and heat input

These results obtained on this procedure allow concluding that:

- The combination of conditions that showed the best results in this work, concerning the UMR, are 100A of Current, approximately 148 J/mm of Heat Input, 81% for deposition efficiency and 24 layers of the AM wall build up;
- The number of layers that represents the best Useful Mass Ratio are 24, corresponding to the Current range of high deposition efficiency and low heat input shown in the chapter 4.1.3;
- The deposition efficiency graph corresponds to a polynomial function, and the inflexion zone represents the transition from short circuit transfer to spray transfer, meaning that the transition of transfer mode affects the metal deposition due the arc instability that occurred [7];
- The heat input corresponds to a polynomial function too, the implications of the heat input on the UMR are:
    - For low heat input the layers melted zone will be not sufficient, creating poor fusion between layers;
    - For high heat input occurs good fusion between layers;

3.4. Hardness

The hardness tests performed in this work were made in order to evaluate the mechanical properties of the AM walls and predict metallurgical aspects.

The hardness tests performed along the AM wall sections of test parts 130A, 110A, 80A and 60A, and its distribution is shown in Figure 8.

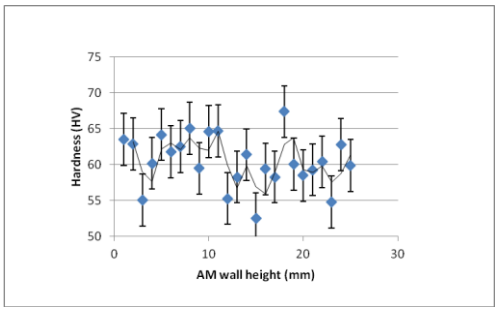

Figure 8: Hardeness distribution along the section of 130A test part

Test part	Heat input (J/mm)	Average Hardness (HV)
130A	0.311	60±3.6
110A	0.220	60.7±3.8
80A	0.148	66.2±4.2
60A	0.089	64.9±2.3

Table 4: Average Hardness of each test part

In all samples a small deviation exists from the average hardness value but the hardness is almost the same in all samples, allowing to conclude that the mechanical properties are homogeneous in all the samples (Table4), despite variations of the Heat Input.

Considering that the nearest average hardness value of the aluminium alloy 5083 is in “O” state is 87HV [106], corresponding to a thermal cycle of annealing and recrystallization, the average values obtained are above this value [109].

Assumptions regarding the average grain size and quantity of precipitates formed during the process can be made, but the metallographic analysis will determine those aspects allowing to achieve solid conclusions.

All values point that the mechanical properties are homogeneous along the AM wall section.

3.5. Microstructure analisys

This microstructure analysis allows to analyse the grain size verify the existence of precipitates by analyzing the chemical composition in different regions. In Figures 9 and 10 is shown the images captured in Light Optical microscopy and SEM/EDS analisys.

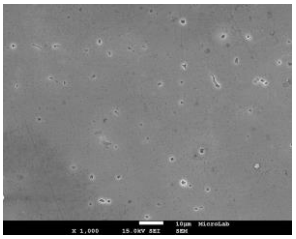

Figure 9: SEM image captured from the 130A test part with 3000x magnification

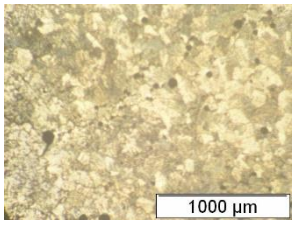

Figure 10: 130A test part microstructure with 50x magnification.

The EDS analysis could be executed in order to differentiate the chemical composition of the dark zones from the bright zones that appeared in the surface scanning. The chemical compositions are represented in table 5:

	Bright Zone		Dark Zone	
Weight percentage	Al (w %)	Mg (w %)	Al (w %)	Mg (w %)
130A	93.35	6.65	93.32	6.68
110A	92.93	7.07	91.18	8.82
80A	92.87	7.13	93.54	6.46
60A	94.61	5.39	91.12	8.88

Table 5: Chemical composition obtained in the EDS analysis, for each test part, concerning the zones of interest.

The approach used in the average grain size determination was the Heyn method which consists in counting 50 grains in a row and measure each one of them in order to determine the average, as shown in Table 6:

Test part	Average grain size (µm)
130A	152 ± 59 µm
110A	157 ± 60 µm
80A	154 ± 56 µm
60A	161 ±51 µm

Table 6: Average grain size for each test part

The average grain size in these samples suffered the same heat treatment that was successive heating and cooling stages [8]. This thermal cycle applied promotes the grain growth and consequently an average grain size that is consistent with the hardness values and is uniform in all samples.

In these samples some pores were found. Pores are a common defect that can be found in welds. In order to validate the AM wall integrity the size and pore fraction were calculated by using a image treatment, *ImageJ,* as shown in Figure 11.

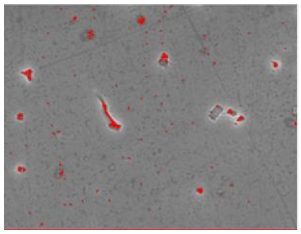

Figure 11: 130A test part with 3000x magnification with the pores highlighted

The results obtained in this brief analysis are expressed by direct data given into *ImageJ*, represented in the table 7:

Test part	Test sample area (µm²)	Average size (µm)	Pores/Sample area (%)
130A	4433	0,057	0,428
110A	4195	0,079	0,416
80A	4589	0,063	0,411
60A	5124	0,048	1,165

Table 7: Porosity analysis considering the occupied area and average size

The results allow to conclude that:

- It was expected to find precipitates in the microstructure of the aluminium, but due the thermal cycle applied , associated with the welding process, precipitates were not formed [9];
- The SEM and EDS analysis allowed to determine the pores formed during the solidification of the alloy. The chemical composition in the dark zones (pores) is nearly the same that in the bright zones;
- The grain size and the lack of precipitates is consistent the average hardness obtained [10].

- The porosity found in the samples does not compromise the mechanical properties because the pore percentage is very low. The preventive measures suggested are [11]:
  - Degrease the surfaces with volatile solvents;
  - Use a wire brush for cleaning after the layer deposition, and the wire brush must be a stainless steel wire brush;
  - Chemical treatment of the surface with alkaline or acid solutions.

3.6. Non Destructive Testing

In this chapter the results obtained in the Non Destructive Tests are presented, on the test parts manufactured at Instituto Superior Técnico and Cranfield University in order to compare with the destructive test results and achieve conclusions about the potential of application of UT in AM.

3.6.1. Non Destructive Testing

The Phased Array Ultrasonic Testing was the first technique used for comparison with other techniques.

These test parts were different from each other regarding the dimensions (Figure 12). The table 8 presents the dimensions for each part tested.

Part number	Thickness (mm)	Width (mm)
1	20	24
2	17	24
3	14	24
4	14	20
5	9	19
6	9	9
7	10	12
8	15	12
9	14	12
10	17	18
11	18	14

Table 8: AM steel parts dimensions

Figure 12: AM steel parts with the respective indication number

The results obtained in this work are represented on a series of zones that were the most relevant for the inspection of manufactured parts. The defects that can be considered as typical or major are the ones that present a signal intensity of 20% or higher, shown on the A-Scan.

Figure 13 represents the layout of the Multi 2000 software, which was used to the PAUT result analysis.

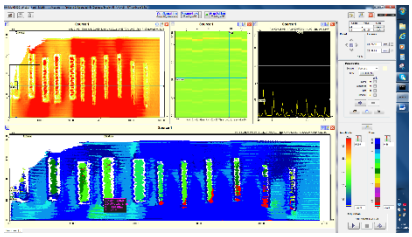

Figure 13: Multi 2000 software display

The parts were analysed individually, and some defects were found in these parts. Figure 14 shows an example of the work developed in a test part.

Part Number	A-Scan	Commentary
4	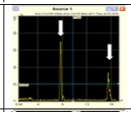	This part presents a major defect near 8mm thickness with intensity near 70% and near 16mm with 35% signal intensity.

Figure 14: PAUT analysis on part 4

The results obtained allow concluding that:

- The PAUT nondestructive test method can be applied at Additive Manufactured parts;
- Analyzed cases, the AM walls were small thus limiting the lateral movement of the probe. This led the lower accuracy of the results in the thinner walls;
- The software data alanyzed provided allows to locate the defect but does not reveal the type of defect or its dimension;

3.6.2. Pulsed echo Ultrasound Testing and Radiation Testing

In the analyzed parts, both for aluminium and steel parts, the results will be expressed mainly by the specters obtained. and the most significant results with the X-Ray acquired.

In UT techniques, the defects that present a signal intensity of 20% or more are the ones that were considered on this work due to the severity of the defects.

The steel test parts were numbered in order to recognize the test results and they are represented in the following Figures 14 and 15.

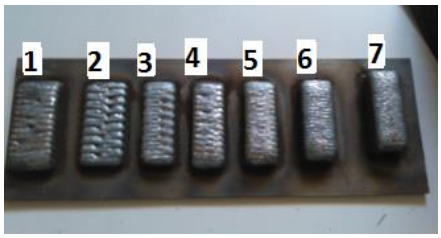

Figure 14: Steel parts for NDT testing numbered from 1 to 7

The dimensions associated to these parts are in Table 9:

Part number	Thickness (mm)	Width (mm)
1	16	44
2	12	45
3	15	35
5	16	33
5	21	34
6	24	34
7	26	34

Table 9: AM steel part dimensions

The analysed aluminium part was the part with the 130A test conditions because it was the only wall with considerable width to be tested with UT technique. The part dimensions are expressed in the Table 4.10:

Test Part	Thickness (mm)	Width (mm)
1A	15	10

Table 10: AM aluminium part dimensions

The IQI (Image Quality Indicator) scheme and the conditions for the radiation tests were the following shown in Table 11.

Test Part Number	Aproximated Thickness (mm)	Minimum IQI	Maximum IQI	Voltage (kV)	Intensity (mA)	Distance from part (mm)	Time (min'seg)
1	24	W11	w13	200	3	700	3'
2	19	W11	w13	200	3	700	2'30
3	22	W11	w13	200	3	700	2'50
4	23	W11	w13	200	3	700	3'10
5	29	W10	w12	200	3	700	4'
6	31	W10	w11	200	3	700	4'20
7	33	W10	w11	200	3	700	5'
1A	39	W9	W12	120	3	700	1'

Table 11: X-Ray testing conditions and IQI obtained

The analisys made in these tests was the direct comparison of the UT spectre and the X-Ray obtained, as shown in Figure 15.

Figure 15: UT spectre for the steel test vs. X-Ray part 1

In summary, the use of NDT in AM parts can be resumed in the following main conclusions:

- UT technique proved a reliable technique in both materials to inspect defects in volume. This method, using the pulsed echo technique, is capable to detect defects in volume through the AM part, although:
  - The UT techniques are developed nowadays to analyse parts with high thicknesses;
  - UT equipment it is pretty simple but the major obstacle during these tests was the lack of records to analyse data after the scan;
- Phased Array Ultrasound testing revealed an excellent first iteration with potential to be studied in different conditions and compared to the other test methods ;
- The defects found were confirmed except the cases when the defects appear on the UT spectres and do not appear in the X-Ray film, due to the low film resolution considering that the IQI was indicated for those cases.

These tests that were performed confirm that UT pulsed echo technique is a feasible solution to analyse AM parts.

4. Conclusions

Additive Manufacturing of Aluminium alloy 5083 components, using CMT process, has been developed during this work. The proposed objectives were achieved and the main conclusions carried are:

1. All tested parameters were able for AM purposes, meaning, all parameters were good to produce wall build ups;
2. The deposition efficiency varies between 85.82% and 76.04%, considering that:
   - Number of layers necessary to build up a wall is lower when the Current is higher;
   - The current and the Wire Feeding Rate have a linear relation due to the excellent thermal

and electrical conductivity of aluminium, reducing the anodic heat to a value near zero;

- The deposition efficiency and the heat input present a quadratic behaviour due to the transfer modes associated to the MIG/MAG process, and the minimum value of deposition efficiency occurs on the current range that corresponds to the short circuit-spray transfer region;

3. The Useful mass ratio study reveals that best conditions for the best results in this study are 100A of current, approximately 148J/mm of Heat Input, 81% of deposition efficiency and 24 layers for the estipulated height of the wall buid up;
   - The number of layers, deposition efficiency and useful mass ration are directly dependent to the heat input of the process:
   - Low heat input values are not enough to melt the material between layers and the poor fusion between layers implies more machining in the final product;
   - High heat input is not recommended because the process stability is compromised and the metal transfer it is not so smooth;
4. The thermal cycle applied during the processing was not enough to ensure that the air cooling was sufficient to produce a fine grain microstructure and enhancing the mechanical properties. On the other hand, the hardness values obtained suggest two important aspects: improved ductility and homogeneous behaviour through all the wall section;
5. The porosity average size and distribution does not interfere significantly with the mechanical properties.
6. The Phased Array Testing and Ultrasound testing results were confirmed by the Radiation testing.

5. References

1. Alcisto, J., Enriquez, A., Garcia, H., Hinkson, S., Steelman, T., Silverman, E., Valdovino, P., Gigerenzer, H., Foyos, J., Ogren, J., Dorey, J., Karg, K., McDonald, T. and Es-Said, O. (2010). Tensile Properties and Microstructures of Laser-Formed Ti-6Al-4V. *Journal of Materials Engineering and Performance*, 20(2), pp.203-212
2. Frazier, W. (2014). Metal Additive Manufacturing: A Review. *Journal of Materials Engineering and Performance*, 23(6), pp.1917-1928
3. Twi-global.com,. 'MIG/MAG – Developments In Low Heat Input Transfer Modes'. N.p., 2015. Web. 25 Apr. 2015.
4. Pickin, C.G., Williams, S.W, M.L., 2011. Characterisation of the cold metal transfer (CMT) process and its application for low dilution cladding. , 211(3), pp.496–502.
5. Nde-ed.org, (2015). Introduction to Ultrasonic Testing. [online] Available at: https://www.nde-ed.org/EducationResources/CommunityCollege/Ultrasonics/Introduction/description.htm [Accessed 15 Sep. 2015].
6. Palani, P. K., & Murugan, N. (2006). Selection of parameters of pulsed current gas metal arc welding. Journal of Materials Processing Technology, 172, 1–10.
7. Sequeira Almeida, P. (2012). *PROCESS CONTROL AND DEVELOPMENT IN WIRE AND ARC ADDITIVE MANUFACTURING*. PhD. Cranfield University.
8. Matweb.com, (2015). MatWeb - The Online Materials Information Resource. [online] Available at: http://www.matweb.com/search/DataSheet.aspx?MatGUID=d105c2a24d6942cdad79259f770fb806&ckck=1 [Accessed 1 Oct. 2015].
9. Gungor, Beytullah et al. 'Mechanical And Microstructural Properties Of Robotic Cold Metal Transfer (CMT) Welded 5083-H111 And 6082-T651 Aluminum Alloys'. *Materials & Design* 54 (2014): 207-211. Web
10. Polmear, I. (2006). Light alloys. Amsterdam: Elsevier/Butterworth-Heinemann.
11. Arc welding of Non Ferrous metals. (2015). 1st ed. Tokyo: Kobe Steel Ltd.